ACS OMEGA

Open Access

http://pubs.acs.org/journal/acsodf

Article

Design, Synthesis, and *In Vitro* Cytotoxic Studies of Some Novel Arylidene-Hydrazinyl-Thiazoles as Anticancer and Apoptosis-Inducing Agents

Ranjana Aggarwal,* Prince Kumar, Suresh Kumar, Rachna Sadana,* Robert Lwanga, Jude Campbell, and Vaishali Chaubal

Cite This: *ACS Omega* 2024, 9, 38832−38845

Read Online

ACCESS | Metrics & More | Article Recommendations | Supporting Information

ABSTRACT: Cancer, defined by uncontrolled cell growth, poses a significant global health challenge, necessitating the development of new anticancer drugs crucial to address drug resistance, side effects, and the need for combination therapies. The study presents the design, synthesis, and anticancer screening of a series of novel functionalized arylidene-hydrazinyl-thiazoles against various human cancer cell lines. The environmentally benign synthetic protocol involves the visible-light prompted, NBS-mediated domino reaction of thiosemicarbazide, heteroaryl aldehydes, and unsymmetrical 1,3-diketones. The regioselective organic transformation delivered the single regioisomeric product, characterized unambiguously through detailed 2D NMR spectral studies. In vitro cytotoxic studies revealed that the synthesized derivatives exhibited excellent cytotoxic potential against BxPC-3, MOLT-4, and MCF-7 cancer cell lines. Notably, compounds **4m**, **4n**, and **4r** showed significant cytotoxicity, reducing cell survival to 23.85−26.45% for BxPC-3, 30.08−33.30% for MOLT-4, and 44.40−47.63% for MCF-7 at a concentration of 10 μM. These compounds profoundly induced apoptosis, evidenced by increased caspase-3/7 activity, loss of mitochondrial membrane potential, and modulation of Bcl2 and Bax gene expression. Additionally, these compounds caused robust cell cycle arrest at the G_2/M phase by inhibiting tubulin polymerization, indicating their multifaceted impact on cancer cells.

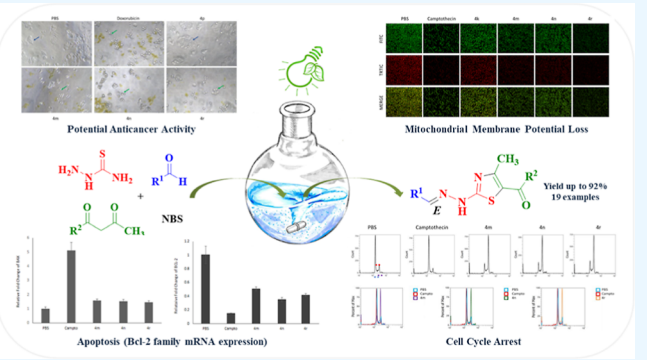

INTRODUCTION

Cancer, a multifaceted and widespread group of diseases marked by uncontrolled cell growth and metastatic potential, poses a significant contemporary healthcare challenge. With diverse malignancies exhibiting unique biological features, cancer ranks as the second leading global cause of mortality, imposing a profound burden on individuals, families, and societies.[1,2] Despite conventional treatments like surgery, chemotherapy, and radiotherapy, which have extended survival and induced remission in many cases, their efficacy is often compromised by significant side effects, necessitating a delicate balance between treatment benefits and patient well-being. In recent years, the landscape of cancer treatment has evolved significantly, with the emergence of targeted therapies, immunotherapies, and precision medicine. Biological therapies, hormonal treatments, and immunomodulatory agents have expanded the therapeutic arsenal, providing additional avenues for personalized and targeted cancer care.[3,4] As researchers and clinicians continue to explore novel chemotherapeutic avenues, the overarching goal remains clear: to develop effective and well-tolerated chemotherapeutic drugs that not only combat cancer at its core but also enhance the quality of life for individuals facing this formidable diagnosis.

Medicinal chemists focus on nitrogen-containing heterocyclic compounds; aza-heterocycles, constituting over 60% of new medications and play a crucial role in anticancer research due to their adaptable and dynamic core scaffold.[5−7] Among aza-heterocycles, thiazole derivatives are the most prevalent and significant heterocyclic molecules that have a high degree of structural diversity, exhibiting fundamental properties in a variety of pharmacological drugs such as alpelisib and dasatinib (anticancer), abafungin and ravuconazole (antifungal), cefdinir (antibiotic), fanetizole (anti-inflammatory) Figure 1, and naturally important compounds (thiamine; vitamin B1).[8−13] The majority of thiazole fragments present in most marketed pharmaceuticals, along with their intrinsic versatility and unique physicochemical properties, have positioned them as true cornerstones of medicinal chemistry.[14−16]

Received: May 25, 2024
Revised: July 3, 2024
Accepted: August 2, 2024
Published: September 3, 2024

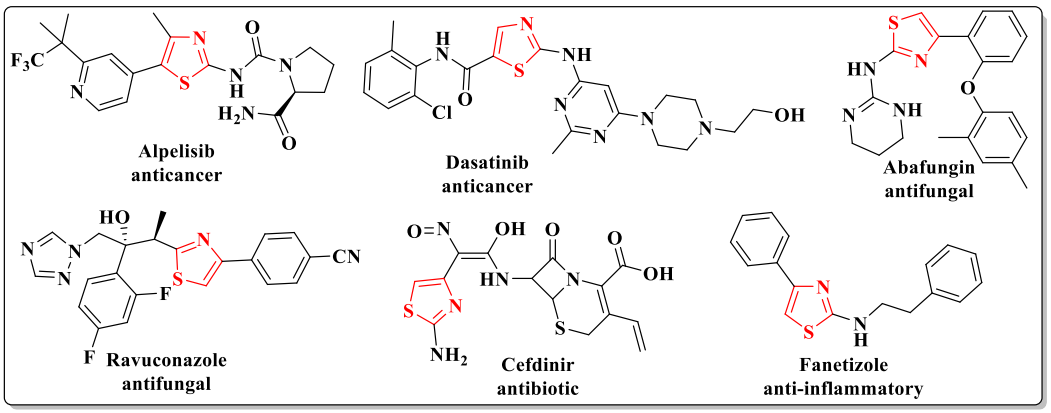

Figure 1. Marketed drugs containing a thiazole scaffold.

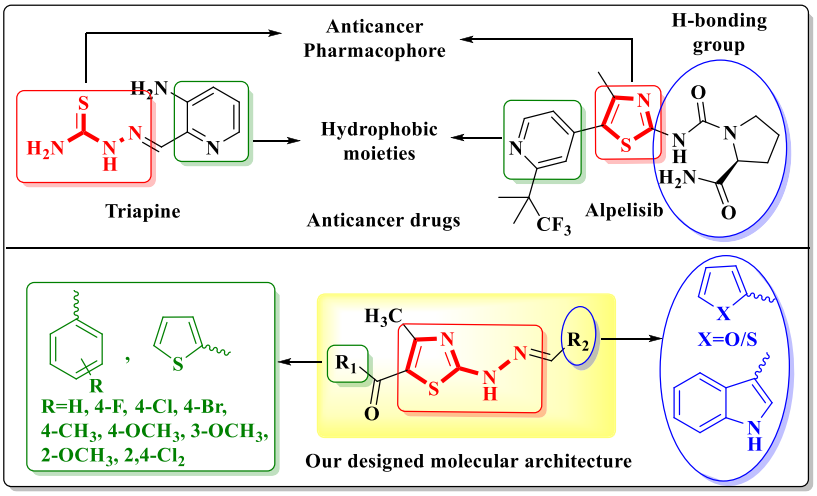

Figure 2. Rationale of drug design.

Thiosemicarbazones and related bioisosteres are frequently found in a wide variety of biologically active substances, such as thioacetazone (an oral antibiotic for tuberculosis) and methisazone (an antiviral drug used in smallpox virus). Triapine, a thiosemicarbazone derivative, was proven to have strong antitumor efficacy by inhibiting ribonucleotide reductase. It has been used in combination with cytarabine to treat myelodysplastic syndrome and leukemia.[17−19] The ability to induce oxidative stress and ROS-mediated cell damage made them some of the most intriguing antitumor inhibitors. Biological and molecular studies of anticancer thiosemicarbazones revealed that these chemicals target several pathways in cancer cells and offer a great place to start when looking for possible candidates in metastatic cancer.

In recent years, molecular hybridization has emerged as a pivotal strategy in drug design, particularly in the development of novel anticancer agents.[20,21] This approach involves the combination of two or more pharmacophores into a single molecule, enhancing biological activity and improving therapeutic profiles. As discussed earlier, the thiazole scaffold, known for its diverse pharmacological properties, has been extensively explored in medicinal chemistry. When hybridized with hydrazone moieties, which are also recognized for their anticancer potential, the resulting compounds often exhibit synergistic effects that enhance their efficacy against cancer cells.[22−24] This synergy is attributed to the unique interactions of the hybrid molecule with multiple biological targets, leading to improved selectivity and potency. In our previous efforts, we have reported the synthesis of some structural analogues of hydrazinyl-thiazoles substituted with aromatic and heteroaromatic ring (pyridine-2-yl), displaying effective DNA binding strength of pyridine-2-yl analogues compared with the aromatic substituted compounds using computational and in vitro studies.[25] In order to obtain better biological efficacy, herein, we have designed a new series of hybrid arylidene-hydrazinyl-thiazoles tethering diverse heteroaromatic scaffolds prospects as anticancer and apoptotic-inducing agents, using alpelisib (thiazole pharmacophore) and triapine (thiosemicarbazone probe) anticancer medications as lead compounds. Besides these marketed medications, various other thiosemicarbazone and thiazole compounds have also shown anticancer properties through several mechanisms.[15,17,26−28] A hybrid system of anticancer pharmacophore, aylidene-hydrazinyl-thiazole fascinating with multiple H-bond-forming groups (heteroaryl moieties) and hydrophobic groups (aryl rings), has been rationally designed to increase the receptor binding probability of the main core (Figure 2).

Prompted with the above-mentioned facts and in continuation of our research work related to the synthesis of biologically active thiazole compounds,[29,30] herein, some novel thiazole scaffolds have been synthesized through an NBS-mediated domino reaction of thiosemicarbazide **1**, heteroaryl aldehydes **2** and 1,3-diketones **3** under environmentally benign visible-light conditions. The synthesized

https://doi.org/10.1021/acsomega.4c04924
ACS Omega 2024, 9, 38832−38845

Table 1. Optimization of Reaction Solvents Under Visible-Light (LED) Conditions[a]

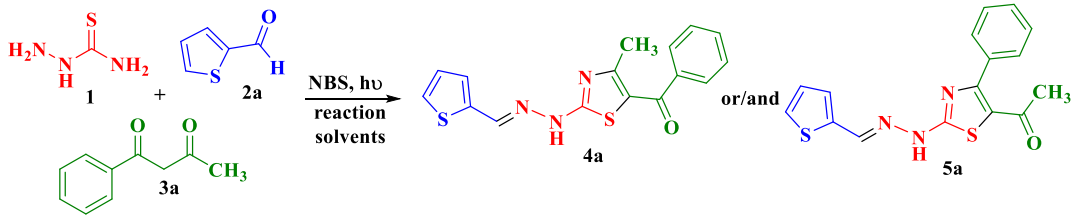

run	solvent	time (h)	yield[b](%)
1	DCM	12	nr
2	DCE	12	nr
3	THF	7	20
4	DMF	8	38
6	MeOH	4	65
7	EtOH	2	82
8	H_2O	3.5	55
9	EtOH/H_2O (1:1)	3	70
10	EtOH/H_2O (2:1)	2	75
11	EtOH/H_2O (3:1)	2	76
12	EtOH/H_2O (**4:1**)	**1.5**	**92**

[a]Reaction of thiosemicarbazide **1** (1.0 mmol), thiophene-2-carbaldehyde **2a** (1.0 mmol), 1-phenylbutane-1,3-dione **3a** (1.0 mmol) and NBS (1.0 mmol) in an appropriate solvent (10 mL) was processed. [b]Isolated yields nr: no reaction.

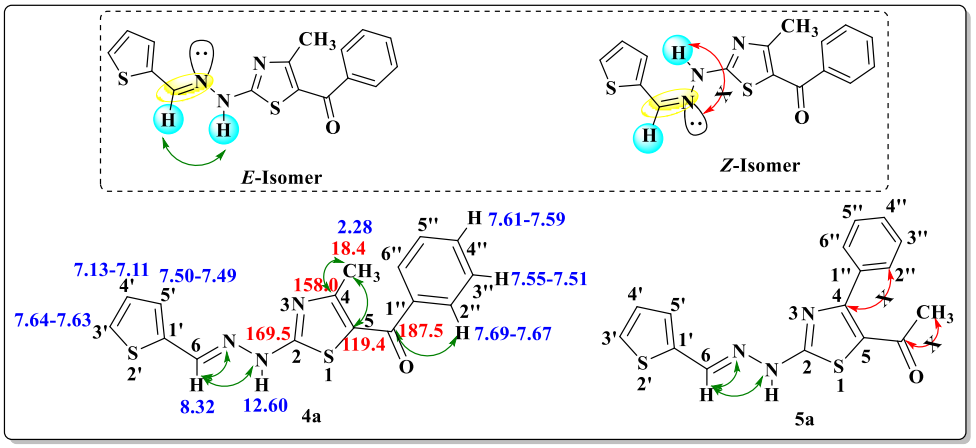

Figure 3. 2D NMR correlations diagram for compound **4a**.

derivatives were thoroughly evaluated for cytotoxicity and apoptosis induction, with systematic assays revealing their effectiveness against diverse cancer cell lines. The study provided valuable insights into the impact of thiazole compounds on cell viability and their potential to initiate cell death. Additionally, the investigation delved into the molecular mechanisms underlying apoptosis induction, enhancing our understanding of the compounds' therapeutic potential in cancer treatment.

RESULT AND DISCUSSION

Chemistry. Taking inspiration from our past work related to visible-light mediated organic transformations,[29] herein, we have synthesized a rationally designed library of arylidene-hydrazinyl-thiazole compounds **4(a-s)** using white LED (Light-emitting diode) as an ecofriendly energy source. Visible-light photocatalysis adds benefits to the reaction conditions such as high yields, economical and easily available energy sources, simple workup processes, ecologically benign reaction conditions, and efficient synthesis with safety and sustainability.

One-pot multicomponent domino approach has been conducted to explore the reactivity of thiosemicarbazide **1**, thiophene-2-carbaldehyde **2a**, phenylbutane-1,3-dione **3a** in the presence of *N*-bromosuccinimide (NBS) in various polar aprotic (dichloromethane (DCM), dichloroethane (DCE), tetrahydrofuran (THF), dimethylformamide (DMF)) and polar protic solvent systems (methanol (MeOH), ethanol (EtOH) and water (H_2O)) under visible-light irradiations (Table 1). However, the best results in terms of reaction period and yields were found with polar protic solvents (MeOH, EtOH and H_2O), particularly in an aqueous ethanol mixture (EtOH/H_2O; 4:1). During the optimization process, thin-layer chromatography (TLC) analysis revealed the formation of a single regioisomeric product, discernible from the two possible outcomes, **4a** or/and **5a**. Subsequent characterization of this product was conducted utilizing advanced analytical techniques including IR, 1D and 2D NMR spectroscopy.

https://doi.org/10.1021/acsomega.4c04924
ACS Omega 2024, 9, 38832−38845

Scheme 1. One-Pot Multicomponent Strategy for the Synthesis of 4

R^1 = a) 2-thienyl, b) 2-furyl, c) 3-indolyl
R^2 = a) Ph, b) 4-MePh, c) 4-OMePh, d) 4-FPh, e) 4-ClPh, f) 4-BrPh, g) 3-OMePh, h) 2-OMePh, i) 2,4-Cl_2Ph, j) 2-thienyl

The ^{1}H NMR spectrum of resulting product **4a/5a** displayed a sharp singlet at δ 2.28 ppm integrated for the three protons consigned to the methyl group and a broad singlet at δ 12.60 ppm integrated for −NH proton. A singlet near to δ 8.32 ppm indicated the −CH of Schiff base linkage, and the aromatic region showed the pattern for thienyl and phenyl ring protons. Besides the required number of aromatic signals, the ^{13}C NMR spectrum showed the signals at δ 187.7 ppm allocated to the carbonyl carbon and δ 18.6 ppm due to the methyl carbon. The IR spectrum further confirmed the presence of −NH, −CO and −C═*N*- group, displaying three distinct absorption bands at 3295, 1642, and 1612 cm^{-1}, respectively. Furthermore, HRMS (ESI) *m*/*z* calculated for $C_{16}H_{13}N_3OS_2$ is 327.0500 and was observed at 328.0498 for $(M + H)^+$ that confirming the successful condensation of reactants to afford targeted arylidene-hydrazinyl-thiazole **4a/5a**.

Ensuring the efficacious condensation to produce arylidene-hydrazinyl-thiazoles, further, the 2D NMR experiments ^{1}H−^{1}H NOESY, (^{1}H−^{13}C) HMBC, (^{1}H−^{13}C) HSQC, (^{1}H−^{15}N) HMBC and (^{1}H−^{15}N) HSQC have been carried out to establish the correct regioisomeric structure of the obtained product. ^{1}H−^{1}H NOESY experiment displayed the cross peaks of iminic C−H with N−H protons, indicating that these two protons are in close proximity (Figure 3). The results were obtained only in the case of *E* stereochemistry for the compound.

In (^{1}H−^{13}C) HMBC spectrum cross-peaks of protons of a methyl group (δ 2.28 ppm) with C-4 (δ 158.0 ppm) and C-5 (δ 119.4 ppm), confirming the presence of methyl substituent at fourth position of thiazole nucleus. Likewise, carbonyl carbon at δ 187.5 ppm displayed a cross peak with H2″/H6″ (δ 7.69−7.67 ppm) protons of the aryl ring indicating the presence of carbonyl carbon with aryl/heteroaryl ring. The possibility of structure **5a** can be ruled out, as there is no correlated peak of carbonyl carbon to methyl protons in the HMBC spectrum. Thus, from the above 2D NMR evidence, the structure can unequivocally be assigned to *(E)*-(4-methyl-2-(2-(thiophen-2-ylmethylene)hydrazinyl)thiazol-5-yl)-(phenyl)methanone **4a** (Figure 3). The 2D NMR correlation results obtained for compound **4a** are presented in the Supporting Information (Table S2).

Following the establishment of optimal circumstances and correct regioisomeric structure, the extent of the devised protocol was investigated under optimized conditions utilizing differently substituted unsymmetrical *β*-diketones **3(a-j)** and heteroaryl aldehydes **2(a-c)** (Scheme 1). All of the reaction combinations proceeded smoothly and produced targeted products **4(a-s)** with high regioselectivity and excellent yields (Table S1). The presence of electron-releasing or electron-drawing groups on diketone did not appear to affect reaction yields.

Biological Activity. *In Vitro Cytotoxic Activity.* Synthesized arylidene-hydrazinyl-thiazoles **4(a-s)** were subjected to in vitro assessment for their cytotoxicity against a panel of five cancer cell lines; human breast cell lines (BT-474 and MCF-7), human pancreatic cancer cell lines (BxPC-3), leukemia cell line (MOLT-4), and lung carcinoma cell line (A-549). We screened all analogues at 10 μM concentration against five different cancer cell lines, and the results are summarized in Table 2. After analysis of the data presented, it was concluded that arylidene-hydrazinyl-thiazoles exhibited moderate to excellent cytotoxicity. Among them, compounds **4b**, **4g**, and **4q** displayed a moderate level of cytotoxic activity. Particularly, the three noteworthy compounds **4m**, **4n**, and **4r** demonstrated outstanding activity, with a remarkable range of percentage cell survival against the tested cancer cell lines: BxPC-3 (23.85−26.45%), MOLT-4 (30.08−33−30%), MCF-7 (44.40−47.63%), BT-474 (53.20−63.97%), and A-549 (55.72−57.09%). The results distinctly indicate that the presence of 2-thienyl and 3-indolyl render compounds potential cytotoxic agents. Remarkably, the 3-indolyl nucleus emerges as particularly effective in this regard. Moreover, a noteworthy revelation from the data is that the presence of an unsubstituted aroyl group **(4m)** or the inclusion of a chloro or methyl-substituted benzoyl group **(4g**, **4r**, **4b**, and **4n)** at the second position of the thiazole ring groups results in an enhancement of cytotoxic potency. These observations underscore the pivotal role of specific structural modifications in influencing cytotoxicity.

Based on the analysis of cell survival data, compounds **4m**, **4n**, and **4r** were selected for further calculation of IC_{50} values presented in Table 3 as they exhibited promising cytotoxic activity. The data indicated that these compounds induce dose-dependent cytotoxicity across all five cancer cell lines. Notably, **4m** exhibits remarkable efficacy with IC_{50} values ranging from 1.69 to 2.2 μM, underscoring its potent cytotoxicity against diverse cancer cell types. Additionally, compounds **4n** and **4r** also demonstrate significant cytotoxic effects, albeit with slightly higher IC_{50} values compared to those of **4m**. Notably, the cytotoxicity of these compounds is comparable to that of doxorubicin (IC_{50} 0.183−0.5 μM), a commonly used chemotherapy drug, across the same panel of cancer cell lines, highlighting their promising therapeutic potential. Data analysis for IC_{50} experiments is provided in Supporting Information Figure S1.

Apoptosis, or programmed cell death, is a vital biological process maintaining tissue homeostasis, embryonic development, and eliminating abnormal cells.[31,32] Unlike necrosis, which results from external factors like trauma, apoptosis is a controlled process by a cascade of molecular events.[33,34] Assessing compounds' ability to induce apoptosis in cancer cells is crucial for identifying potential anticancer agents. Herein, compounds **4m**, **4n**, and **4r** were selected to be used

https://doi.org/10.1021/acsomega.4c04924
ACS Omega 2024, 9, 38832−38845

Table 2. In Vitro Screening of Arylidene-Hydrazinyl-Thiazoles Expressed as Percentage Cell Survival Values ± Standard Deviation from Three Replicates

Comp.	R^1	R^2	% Cell Survival				
			MCF-7	BT-474	A-549	MOLT-4	BxPC-3
Buffer			100.00±3.06	100.00±9.71	100.00±11.9	100.00±15.48	100.00±12.0
4a	2-thienyl	Ph	76.43±17.48	138.34±36.8	86.96±9.58	71.44±20.61	74.70±7.04
4b	2-thienyl	4-MePh	68.12±12.60	85.90±23.60	76.20±10.66	50.34±8.86	40.29±7.00
4c	2-thienyl	4-OMePh	77.00±10.85	122.89±33.9	81.18±9.43	65.30±11.09	79.33±14.37
4d	2-thienyl	4-FPh	71.63±16.36	113.11±41.5	87.16±9.00	61.18±15.44	78.79±16.35
4e	2-thienyl	4-ClPh	74.59±12.13	116.92±32.9	80.05±4.46	45.24±10.84	90.80±16.11
4f	2-thienyl	4-BrPh	103.71±7.35	103.55±24.0	89.21±7.90	85.59±16.34	99.85±11.50
4g	2-thienyl	2,4-Cl_2Ph	50.84±11.79	75.17±20.01	72.69±6.73	52.77±10.97	58.70±4.24
4h	2-thienyl	2-thienyl	81.42±19.07	89.88±14.99	84.29±6.16	92.77±10.87	99.14±9.51
4i	2-furyl	Ph	85.80±8.60	99.29±13.05	83.54±6.48	90.13±13.35	81.06±8.87
4j	2-furyl	4-MePh	86.87±8.07	87.52±21.70	79.65±7.22	74.81±17.76	94.67±9.01
4k	2-furyl	4-OMePh	71.10±7.34	104.04±24.7	77.01±4.68	72.08±22.03	86.09±30.66
4l	2-furyl	2,4-Cl_2Ph	76.85±23.71	101.10±25.8	75.70±7.13	70.64±9.88	77.45±8.07
4m	3-indolyl	Ph	44.40±8.83	63.97±16.86	55.72±5.38	32.16±5.10	23.85±4.44
4n	3-indolyl	4-MePh	46.34±11.13	56.29±8.53	57.09±8.92	33.30±8.49	26.02±3.48
4o	3-indolyl	2-OMePh	74.06±17.84	99.84±21.74	90.03±8.01	63.79±19.91	83.31±16.24
4p	3-indolyl	3-OMePh	81.57±13.75	118.33±23.5	92.03±3.98	73.48±9.62	93.58±10.31
4q	3-indolyl	4-FPh	50.09±12.50	91.26±8.72	64.43±10.56	50.63±8.38	32.85±2.00
4r	3-indolyl	4-ClPh	47.63±14.44	53.20±7.66	56.17±7.55	30.08±5.66	26.45±3.22
4s	3-indolyl	2,4-Cl_2Ph	73.12±21.16	94.60±13.84	84.83±5.43	43.68±21.17	78.63±33.21
DOXO			48.20±6.57	51.61±6.43	41.98±5.23	10.29±1.12	11.55±3.53

throughout this study for in-depth investigation based on their promising cytotoxic potential, suggesting their potential utility as lead candidates for the development of novel anticancer agents.

Morphological Analysis of MCF-7 Cancer Cell Line. Apoptosis exhibits distinct morphological and biochemical changes in cells, including cell shrinkage, membrane blebbing, chromatin condensation, nuclear fragmentation, and formation of apoptotic bodies. Morphological analysis is crucial for evaluating the apoptosis-inducing properties of compounds, involving microscopic examination of cellular structures to detect these characteristic changes.[35,36] In order to investigate

https://doi.org/10.1021/acsomega.4c04924
ACS Omega 2024, 9, 38832−38845

Table 3. Determination of IC_{50} Values of Selected Arylidene-Hydrazinyl-Thiazoles

compound	cancer cell lines (IC50, μM ± SD)				
	MCF-7	BT-474	A-549	MOLT-4	BxPC-3
4m	1.82 ± 0.158	1.9 ± 0.17	2.2 ± 0.10	1.69 ± 0.897	1.71 ± 0.635
4n	5.76 ± 0.853	4.8 ± 0.55	4.3 ± 0.43	5.24 ± 0.115	4.14 ± 0.458
4r	1.59 ± 1.60	2.1 ± 0.11	1.5 ± 0.11	3.02 ± 1.94	3.42 ± 1.53
doxorubicin	0.183 ± 0.005	0.5 ± 0.12	0.2 ± 0.05	0.206 ± 0.143	0.380 ± 0.100

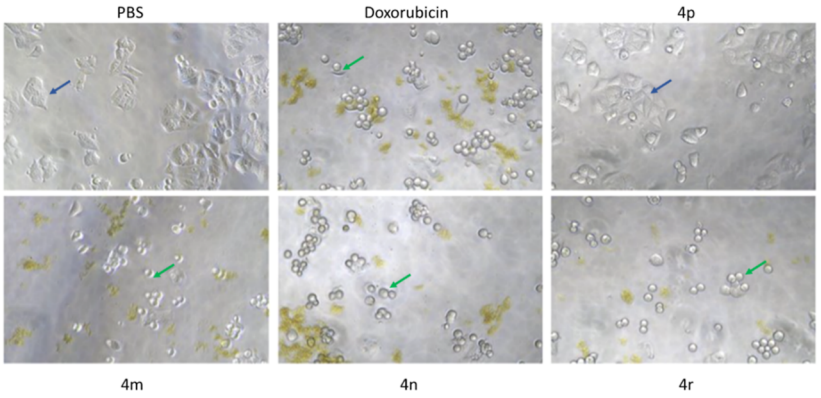

Figure 4. Phase contrast images of MCF-7 cells treated with 5 μM of **4m, 4n, 4r**, and **4p**. Green arrow: swelling and cell membrane lysis induced by **4m**, **4n**, and **4r** and doxorubicin are indicated by green arrow. Normal morphology for untreated cells or treated with noncytotoxic compound **4p** is indicated with blue arrow.

the potential impact of these compounds (**4m**, **4n**, and **4r**) and noncytotoxic compound **4p** on cellular viability and apoptosis induction, MCF-7 cells were treated with compounds **4m**, **4n**, and **4r** at a final concentration of 5 μM for 24 h. Following treatment, morphological changes were meticulously examined using a phase contrast microscope, Figure 4.

It can be inferred that the treatment with these compounds (**4m**, **4n**, and **4r**) results in significant alterations in cellular morphology including reduced cell confluence, plasma membrane blebbing, and a noticeable decrease in structural integrity. These morphological changes strongly suggest the potential for compromised cell viability and the initiation of apoptotic processes. For comparative purposes, Doxorubicin was employed as a positive control to validate the observed morphological changes induced by the tested compounds. However, the noncytotoxic compound **4p** did not elicit similar morphological alterations.

Notably, while these compounds effectively induced apoptosis in MCF-7 cells, their impact on the viability of MCF10A cells was markedly lower when compared to untreated controls (data provided in Supporting Information, Figure S2). These findings highlight the selective cytotoxicity of compounds **4m**, **4n**, and **4r** toward cancerous cells, particularly MCF-7 cells, while demonstrating minimal effects on normal MCF10A cells. This distinctive variance in cytotoxicity underscores the potential utility of compounds **4m**, **4n**, and **4r** as promising candidates for further development as cancer therapeutics.

Induction of Apoptosis via an Intrinsic Apoptosis Pathway. *Caspase-3/7 Assay.* Caspase-3 and caspase-7 are key protease enzymes driving the biochemical and morphological changes of apoptosis, including chromatin condensation, DNA fragmentation, cell shrinkage, and membrane blebbing, marking the execution phase. Caspase-3 and caspase-7 are effector caspases that act downstream in the apoptotic pathway, cleaving various cellular substrates and ultimately leading to cell death. Measuring caspase-3/7 activity provides valuable insights into the progression and extent of apoptosis within a cell population. Various techniques are employed to measure caspase-3/7 activity, typically involving the cleavage of specific fluorogenic or luminescent substrates by active caspase-3/7 enzymes within the cell. Upon cleavage, these substrates emit fluorescent or luminescent signals, which can be quantified to provide a direct readout of caspase-3/7 activity.

To investigate the potential of compounds **4m**, **4n**, and **4r** to induce apoptosis in MOLT-4 leukemia cells, the cells were treated with these compounds and subsequently, caspase-3/7 activity was measured.[37] As depicted in Figure 5, the treated cells displayed a remarkable approximately two-fold increase in fluorescence intensity compared to the control cells treated with PBS. This elevation in fluorescence suggests a significant upsurge in caspase 3/7 activity, indicating the activation of

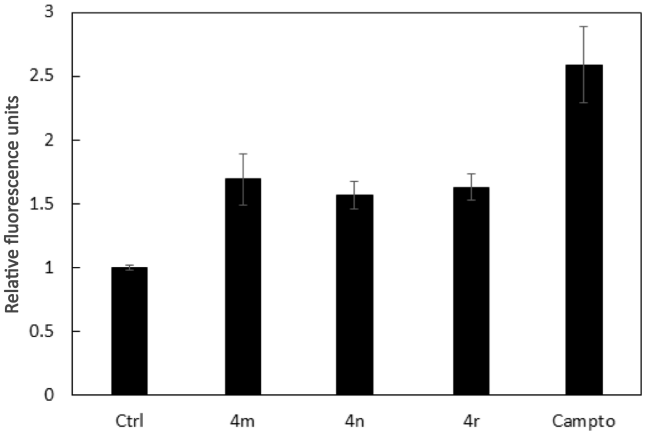

Figure 5. Caspase-3/7 activation-induced by **4m**, **4n**, and **4r** in MOLT-4 leukemia cells.

https://doi.org/10.1021/acsomega.4c04924
ACS Omega 2024, 9, 38832−38845

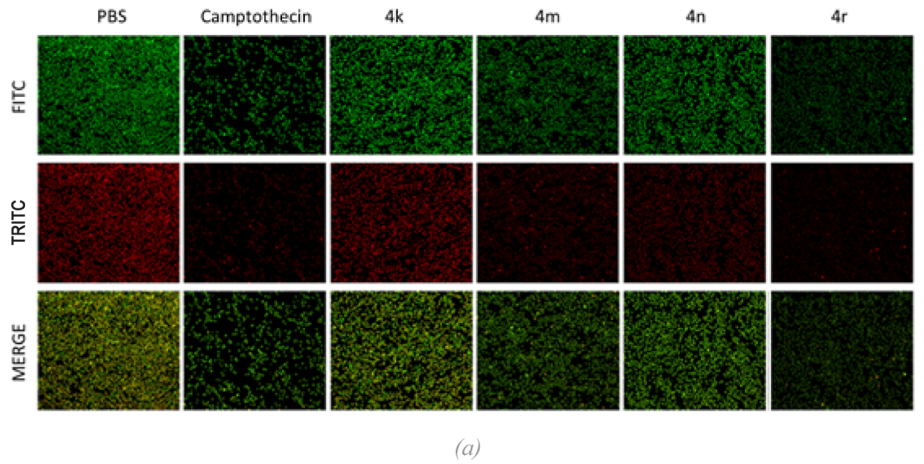

(a)

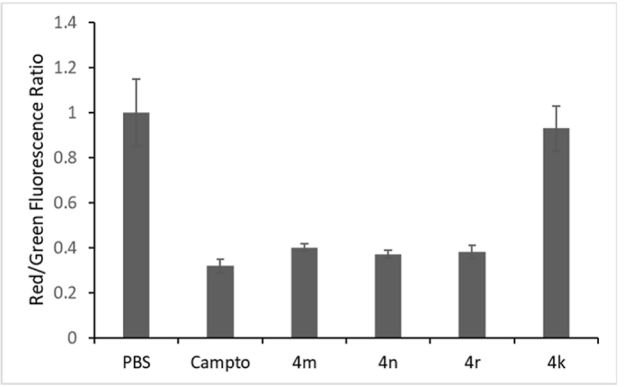

(b)

Figure 6. Investigating mitochondrial membrane potential loss in MOLT-4 cells. (a) Comparison of red fluorescence alteration with **4m**, **4n**, **4r**, **4k**, and camptothecin treatment. (b) Quantitative evaluation of the ratio of red/green fluorescence.

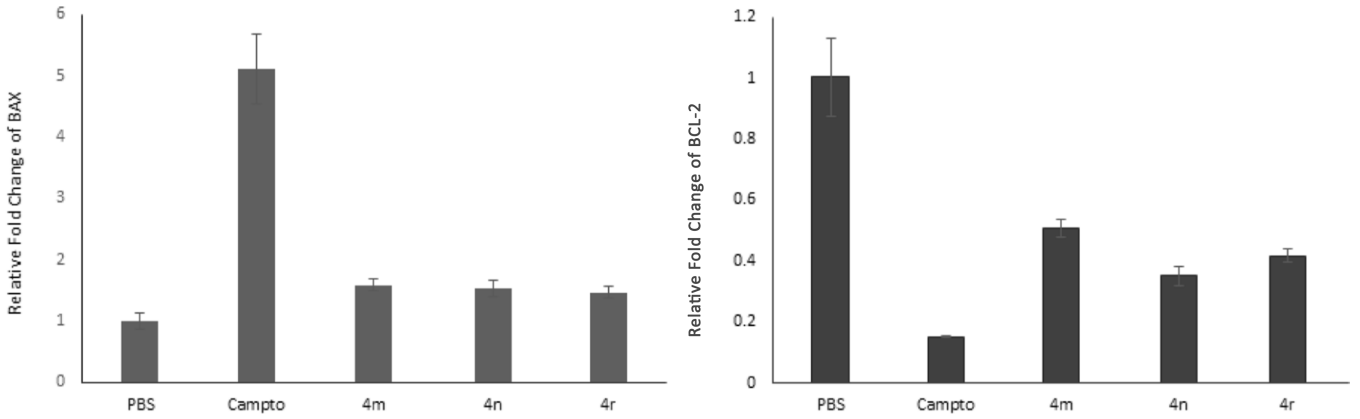

Figure 7. Examining pro- and antiapoptotic gene expression in MCF-7 cells through RT-PCR.

apoptotic pathways by compounds **4m**, **4n**, and **4r** within the MOLT-4 leukemia cell population. In this study, camptothecin was employed as a positive control. This natural alkaloid, derived from *Camptotheca acuminata*, is renowned for its potent apoptotic-inducing properties, exerting its effects through the inhibition of topoisomerase I, leading to DNA damage and subsequent apoptotic cell death.[38]

Assessment of Mitochondrial Membrane Loss. The disruption of normal mitochondrial function, especially alterations impacting the mitochondrial membrane potential ($\Delta\Psi m$), is a distinctive hallmark of apoptosis.[39,40] Changes in $\Delta\Psi m$ signify mitochondrial dysfunction, which can trigger apoptotic signaling cascades, leading to cell death. To investigate whether cytotoxic compounds **4m**, **4n**, and **4r**, along with a noncytotoxic compound **4k** (for comparative purposes), induce apoptosis through the loss of mitochondrial membrane potential, MOLT-4 cells were treated with 3 μM of the respective compounds and incubated for 24 h. After incubation, cells were stained with JC-10 (a dye that fluoresces at two different wavelengths based on its conformational state) for visualization through fluorescence microscopy in the FITC channel at 235 nm exposure and the TRITC channel at 670 nm exposure. The results revealed that cells treated with **4m**, **4n**, **4r**, and camptothecin displayed a decrease in JC-10 (red)

https://doi.org/10.1021/acsomega.4c04924
ACS Omega 2024, 9, 38832−38845

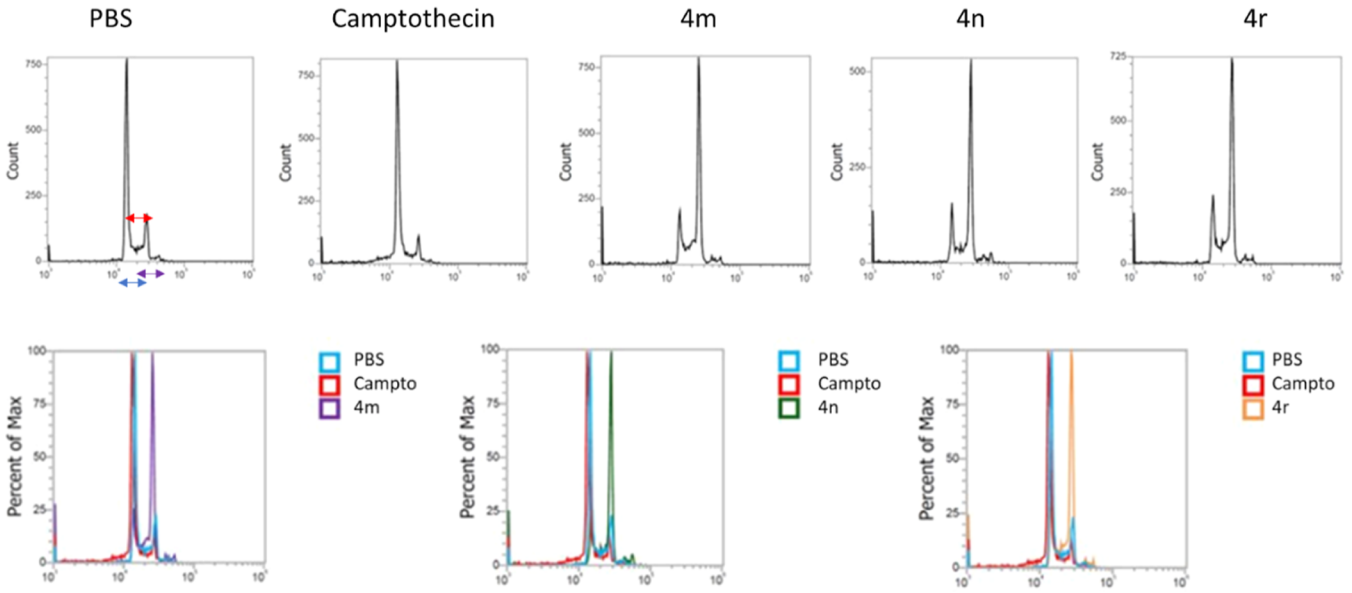

Figure 8. Investigating cell cycle progression in MOLT-4 cancer cells using flow cytometry. (Top panel) Flow cytometry analysis of MOLT-4 cells treated with PBS, camptothecin, **4m**, **4n**, and **4r** for 24 h. (Bottom panel) Overlay of data from PBS (negative control), a test compound (either **4m**, **4n**, or **4r**), and camptothecin (positive control)-treated cells.

fluorescence, indicating a loss of mitochondrial membrane potential (Figure 6a). Crucially, no reduction in fluorescence was observed when cells were treated with either PBS or a noncytotoxic compound **4k**. These findings strongly suggest that the mentioned compounds induce apoptosis by causing dysregulation of the mitochondria; a phenomenon frequently associated with intrinsic apoptosis.

Furthermore, to quantify the altered mitochondrial membrane potential of cells upon treatment with **4m**, **4n**, **4r**, and **4k**, ratio of red/green fluorescence, indicative of dye aggregates and monomers, was calculated. A reduction in the ratio of aggregates to monomers in treated cells (Figure 6b) was observed, indicating the loss of mitochondrial membrane potential, suggesting the occurrence of apoptosis.

Analysis of Bcl-2 Family mRNA Expression in MCF-7 Cells. To further substantiate the involvement of mitochondria in the induction of apoptosis by **4m**, **4n**, and **4r** in MCF-7 cells, we conducted qRT-PCR analysis to assess the mRNA expression levels of key Bcl-2 family members; specifically, Bax (a pro-apoptotic protein) and Bcl-2 (an antiapoptotic protein).[41] These proteins play crucial roles as mediators in the mitochondrial apoptotic pathway. As illustrated in Figure 7, treatment with these three cytotoxic compounds resulted in a significant 1.5-fold increase in the expression levels of pro-apoptotic protein Bax compared with untreated cells. Concurrently, these compounds effectively reduced the expression levels of the antiapoptotic protein Bcl-2 when compared to control cells. The collective findings suggest that treatment with **4m**, **4n**, and **4r** led to an elevation in the expression levels of pro-apoptotic protein, accompanied by a simultaneous reduction in the expression of antiapoptotic protein in MCF-7 cells. This observed pattern closely mirrors the effects seen in cells treated with camptothecin, a well-known apoptotic-inducing agent, further reinforcing the notion that compounds **4m**, **4n**, and **4r** exert their apoptotic effects via mitochondria-mediated pathways.

Cell Cycle Arrest Measured by Flow Cytometry in MOLT-4 Cells. Cell cycle arrest, a crucial cellular process regulating cell proliferation and DNA replication, can be effectively evaluated by using flow cytometry. This technique allows for the quantitative analysis of individual cells based on their DNA content, enabling the identification of distinct phases of the cell cycle, such as G_o (quiescent stage), G_1 (cell growth), S (DNA synthesis), G_2 (cell growth), and M (mitosis) phases. By analyzing the distribution of cells within these phases, flow cytometry provides valuable insights into the progression or arrest of the cell cycle in response to various stimuli or treatments. This approach facilitates the elucidation of mechanisms underlying cell cycle regulation and aids in the characterization of potential therapeutic agents that target cell cycle progression. In our study, to investigate whether alterations in the cell cycle distribution were responsible for MOLT-4 cell growth inhibition and apoptosis induction or not, the population of MOLT-4 cells in different cell cycle phases was quantified by flow cytometry following treatment with 5 μM of **4m**, **4n**, and **4r**. Interestingly, treatment with camptothecin led to the accumulation of cells at the G_o/G_1 phase compared to that of untreated cells. In contrast, treatment with **4m**, **4n**, and **4r** resulted in the accumulation of cells in the G_2/M phase (Figure 8).

Tubulin Polymerization Inhibition Assay. Inhibition of tubulin polymerization is a significant mechanism in the identification and development of anticancer agents. Tubulin is a structural protein that polymerizes to form microtubules, which are essential components of the cytoskeleton and are crucial for cell division. Microtubules play a critical role in mitosis, the process of cell division that ensures the proper segregation of chromosomes into daughter cells. Disruption of microtubule dynamics can lead to cell cycle arrest and apoptosis (programmed cell death), making it a valuable target for anticancer therapy. To investigate whether the antiproliferative activities of potent compounds **4m**, **4n**, and **4r** involve interactions with tubulin, a potential molecular target in the G_2/M phase of cell cycle, these compounds were tested for tubulin inhibition activity in a cell-free in vitro assay. The results demonstrated that the addition of compounds **4m**, **4n**,

https://doi.org/10.1021/acsomega.4c04924
ACS Omega 2024, 9, 38832−38845

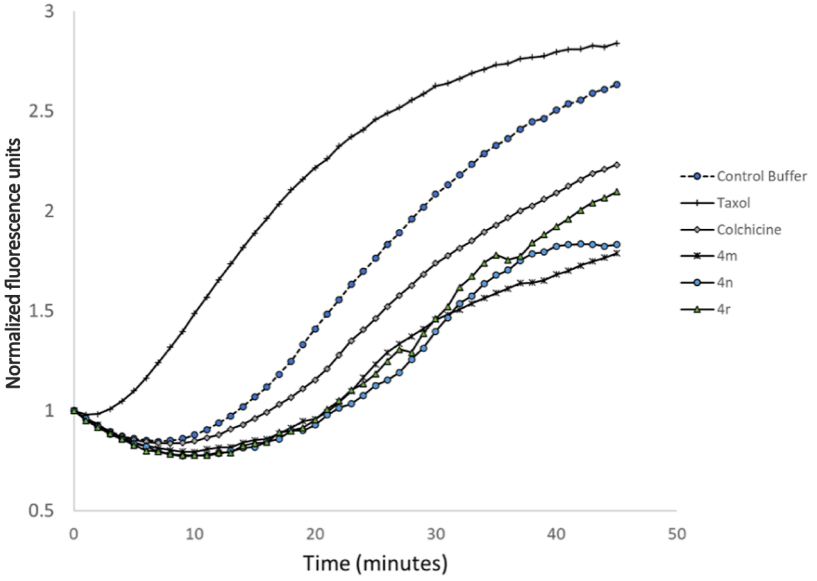

Figure 9. Dose-dependent inhibition of tubulin polymerization by compounds **4m**, **4n**, and **4r**. Colchicine was used as a positive control.

and **4r** caused a decrease in tubulin polymerization in a dose-dependent manner, as shown in Figure 9. This effect was comparable to that observed with colchicine, a well-known tubulin inhibitor, confirming that compounds **4m**, **4n**, and **4r** effectively inhibit microtubule formation. Taclitaxel was used to demonstrate how it stabilized tubulin polymerization.

CONCLUSIONS

In conclusion, we have developed a new and efficient method for synthesizing a range of arylidene-hydrazinyl-thiazoles **4** through multicomponent Hantzsch thiazole [3 + 2] condensation of thiosemicarbazide **1**, heteroaryl aldehyde **2**, and 1,3-diketones **3**, in the presence of NBS using aqueous ethanol under visible-light irradiations. The synthetic methodology is particularly noteworthy for its sustainability as it does not require the use of metals or additives in the cyclocondensation reaction and employs a completely environmentally friendly reaction medium and green energy source. In vitro, cytotoxic studies revealed that the synthesized derivatives exhibited excellent cytotoxic potential against BxPC-3, MOLT-4, and MCF-7 cancer cell lines, which could induce apoptosis and interference with the cell cycle. Notably, compounds **4m**, **4n**, and **4r**, unveiled significant cytotoxicity, resulting in notable reductions in cell survival against BxPC-3 (23.85−26.45%), MOLT-4 (30.08−33−30%), and MCF-7 (44.40−47.63%) at a concentration of 10 μM. These compounds displayed a profound induction of apoptosis, as evidenced by increased caspase-3/7 activity, loss of mitochondrial membrane potential, and modulation of Bcl2 and Bax gene expression. Additionally, they induced robust cell cycle arrest in the G_2/M phase by inhibiting tubulin polymerization, suggesting a multifaceted impact on cancer cells. These findings position compounds **4m**, **4n**, and **4r** as promising candidates for further exploration and potential development as advanced therapeutic agents against various malignancies.

EXPERIMENTAL SECTION

Melting points in open capillaries were examined using an electrical digital Melting Point Apparatus and are uncorrected. Merck Kieselgel 60 F254 silica gel plates were used for analytical TLC, and they were seen under UV light (254 nm). A JNM-ECZ400S/L1 instrument was used to record the ^{1}H (400 MHz) and ^{13}C NMR (100 MHz) spectra in DMSO-d_6 for analytical purposes. The chemical shifts are expressed in parts per million (ppm), and the coupling constant J is expressed in Hz with TMS as the internal standard. 2D correlation spectroscopy, (^{1}H−^{13}C) gs-HSQC, (^{1}H−^{13}C) gs-HMBC, (^{1}H−^{15}N) gs-HSQC, (^{1}H−^{15}N) gs-HMBC, and ^{1}H−^{1}H NOESY of the samples were performed at Kurukshetra University in Kurukshetra. The IR spectra were recorded on a Buck Scientific IR M-500 spectrophotometer in KBr pellets (ν_{max} in cm^{-1}). HRMS were measured in the ESI + mode at the SAIF, Punjab University, Chandigarh.

The 1,3-diketones were synthesized using methods described in the literature.[25,42] Commercially available thiosemicarbazide (Avra Chemicals, India), aldehydes (Himedia, India), and NBS (Avra Chemicals, India) were used without any purification.

General Method for the Synthesis of 5-Aroyl-4-methyl-2-arylidene-hydrazinyl-thiazoles 4(a-s). In a 50 mL Erlenmeyer flask, a mixture of thiosemicarbazide **1** (0.91 g, 1.0 mmol), heteroaryl aldehydes **2(a-c)** (1.0 mmol), 1,3-diketones **3(a-j)** (1.0 mmol), and NBS (0.178 g,1.0 mmol) was stirred in aqueous ethanol (EtOH/H_2O; 4:1) under visible-light irradiations (white LED) for about 1−2 h. After completion, the reaction was monitored by TLC using ethyl acetate: petroleum ether (60:40, v/v) as the eluent, and the solvent was evaporated under reduced pressure using a rotatory evaporator. The gummy mass was treated with a saturated aqueous solution of sodium bicarbonate and extracted with ethyl acetate, slow evaporation of the solvent gave the desired product, separated by filtering, and rinsed with aqueous ethanol (25%). After being dried and recrystallized from EtOH, the product produced high quantities of pure arylidene-hydrazinyl-thiazoles **4(a-s)**. The IR, 1D, and 2D NMR and HRMS techniques were used to characterize the products.

(E)-(4-methyl-2-(2-(thiophen-2-ylmethylene)hydrazinyl)-thiazol-5-yl)(phenyl)methanone (4a). Brown Solid. mp. 174

https://doi.org/10.1021/acsomega.4c04924
ACS Omega 2024, 9, 38832−38845

°C; yield: 92%; IR (KBr) ν_{max} (cm^{-1}): 1574 (C═O), 1612 (C═N), 3348 (N−H);

^{1}H NMR (400 MHz, DMSO-d_6) δ 12.60 (s, 1H, −NH), 8.32 (s, 1H, 6-CH), 7.69−7.67 (m, 2H, 2″,6″-H), 7.64−7.63 (m, 1H, 3′-H), 7.61−7.59 (m, 1H, 4″-H), 7.55−7.51 (m, 2H, 3″,5″-H), 7.50−7.49 (dd, 1H, J = 3.6 Hz, J = 0.9 Hz, 5′-H), 7.13−7.11 (dd, 1H, J = 5.0 Hz, J = 3.6 Hz, 4′-H), 2.28 (s, 3H, 4-Me).

^{13}C NMR (101 MHz) δ: 187.5, 169.5, 158.0, 141.2, 140.6, 138.8, 131.9, 130.8, 129.0, 128.8, 128.3, 127.9, 119.4, 18.4.

HRMS (ESI): m/z calcd for $C_{16}H_{13}N_3OS_2$: 327.0500; found: 328.0498 $[M + H]^+$.

(E)-(4-methyl-2-(2-(thiophen-2-ylmethylene)hydrazinyl)-thiazol-5-yl)(p-tolyl)methanone (4b). Creamy White Solid. mp. 182 °C; yield: 88%; IR (KBr) ν_{max} (cm^{-1}): 1566 (C═O), 1636 (C═N), 3280 (N−H);

^{1}H NMR (400 MHz, DMSO-d_6) δ 12.54 (s, 1H, −NH), 8.32 (s, 1H, 6-CH), 7.64−7.63 (d, 1H, ^3J = 4.8 Hz, 3′-H), 7.61−7.59 (d, 2H, ^3J = 8.0 Hz, 2″,6″-H), 7.44−7.43 (d, 1H, ^3J = 2.8 Hz, 5′-H), 7.34−7.32 (d, 2H, ^3J = 8.0 Hz, 3″,5″-H), 7.13−7.11 (dd, 1H, J = 4.8 Hz, J = 3.6 Hz, 4′-H), 2.39 (s, 3H, 4″-Me), 2.29 (s, 3H, 4-Me).

^{13}C NMR (101 MHz) δ 186.7, 169.1, 158.3, 141.7, 140.3, 138.6, 137.6, 130.4, 128.9, 128.7, 127.9, 21.1, 18.1.

HRMS (ESI): m/z calcd for $C_{17}H_{15}N_3OS_2$: 341.0657; found: 342.0653 $[M + H]^+$.

(E)-(4-methoxyphenyl)(4-methyl-2-(2-(thiophen-2-ylmethylene)hydrazinyl)thiazol-5-yl)methanone (4c). Buff Colored Solid. mp. 197 °C; yield: 87%; IR (KBr) ν_{max} (cm^{-1}): 1566 (C═O), 1628 (C═N), 3288 (N−H);

^{1}H NMR (400 MHz, DMSO-d_6) δ 12.50 (s, 1H, −NH), 8.31 (s, 1H, 6-CH), 7.73−7.70 (d, 2H, ^3J = 8.7 Hz, 2″,6″-H), 7.64−7.63 (d, 1H, ^3J = 5.0 Hz, 3′-H), 7.44−7.43 (m, 1H, 5′-H), 7.13−7.11 (dd, 1H, J = 5.0 Hz, J = 3.6 Hz, 4′-H), 7.08−7.05 (d, 2H, ^3J = 8.7 Hz, 3″,5″-H), 3.85 (s, 3H, 4″-OMe), 2.31 (s, 3H, 4-Me).

^{13}C NMR (101 MHz) δ 186.25, 175.74, 169.10, 162.39, 140.73, 138.81, 132.65, 130.67, 130.60, 128.88, 128.26, 113.97, 55.66, 18.36.

HRMS (ESI): m/z calcd for $C_{17}H_{15}N_3O_2S_2$: 357.0606; found: 358.0601 $[M + H]^+$.

(E)-(4-fluorophenyl)(4-methyl-2-(2-(thiophen-2-ylmethylene)hydrazinyl)thiazol-5-yl)methanone (4d). Brownish Solid. mp. 190 °C; yield: 88%; IR (KBr) ν_{max} (cm^{-1}): 1574 (C═O), 1612 (C═N), 3263 (N−H);

^{1}H NMR (400 MHz, DMSO-d_6) δ 12.62 (s, 1H, −NH), 8.32 (s, 1H, 6-CH), 7.80−7.76 (m, 2H, 2″,6″-H), 7.65−7.63 (dt, 1H, J = 5.0 Hz, J = 0.8 Hz, 3′-H), 7.45−7.44 (dd, 1H, J = 3.6 Hz, J = 1.0 Hz, 5′-H), 7.38−7.34 (m, 2H, 3″,5″-H), 7.14−7.11 (dd, 1H, J = 5.0 Hz, J = 3.6 Hz, 4′-H), 2.29 (s, 3H, 4-Me).

^{13}C NMR (101 MHz) δ 185.6, 165.1, 162.6, 138.7, 138.5, 136.8, 130.6, 128.8, 128.0, 115.6, 115.4, 115.2, 18.5.

HRMS (ESI): m/z calcd for $C_{16}H_{12}FN_3OS_2$: 345.0406; found: 346.0403 $[M + H]^+$.

(E)-(4-chlorophenyl)(4-methyl-2-(2-(thiophen-2-ylmethylene)hydrazinyl)thiazol-5-yl)methanone (4e). Creamish White Solid. mp. 201 °C; yield: 90%; IR (KBr) ν_{max} (cm^{-1}): 1574 (C = O), 1651 (C = N), 3285 (N−H);

^{1}H NMR (400 MHz, DMSO-d_6) δ 12.64 (s, 1H, −NH), 8.33 (s, 1H, 6-CH), 7.73−7.70 (m, 2H, 2″,6″-H), 7.65−7.64 (d, 1H, ^3J = 5.0 Hz, 3′-H), 7.61−7.59 (m, 2H, 3″,5″-H), 7.45−7.44 (d, 1H, ^3J = 3.6 Hz, 5′-H), 7.14−7.11 (dd, 1H, J = 5.0 Hz, J = 3.6 Hz, 4′-H), 2.28 (s, 3H, 4-Me).

^{13}C NMR (101 MHz) δ: 185.6, 169.5, 139.0, 138.5, 136.3, 130.6, 129.7, 128.8, 128.6, 128.0, 18.4.

HRMS (ESI): m/z calcd for $C_{16}H_{12}ClN_3OS_2$: 361.0110; found: 362.0106 $[M + H]^+$.

(E)-(4-bromophenyl)(4-methyl-2-(2-(thiophen-2-ylmethylene)hydrazinyl)thiazol-5-yl)methanone (4f). Brownish Solid. mp. 224.5 °C; yield: 85%; IR (KBr) ν_{max} (cm^{-1}): 1558 (C═O), 1605 (C═N), 3263 (N−H);

^{1}H NMR (400 MHz, DMSO-d_6) δ 12.62 (s, 1H, −NH), 8.33 (s, 1H, 6-CH), 7.75−7.72 (d, 2H, ^3J = 8.4 Hz, 2″,6″-H), 7.65−7.63 (m, 3H, 3′,3″,5″-H), 7.45−7.44 (d, 1H, ^3J = 3.6 Hz, 5′-H), 7.14−7.11 (m, 1H, 4′-H), 2.28 (s, 3H, 4-Me).

^{13}C NMR (101 MHz) δ: 185.8, 169.3, 139.3, 138.5, 131.5, 130.6, 129.8, 128.8, 128.0, 125.2, 18.4.

HRMS (ESI): m/z calcd for $C_{16}H_{12}BrN_3OS_2$: 404.9605; found: 405.9600 $[M + H]^+$.

(E)-(2,4-dichlorophenyl)(4-methyl-2-(2-(thiophen-2-ylmethylene)hydrazinyl)thiazol-5-yl)methanone (4g). Creamy Whitish Solid. mp. 201 °C; yield: 86%; IR (KBr) ν_{max} (cm^{-1}): 1551 (C═O), 1597 (C═N), 3178 (N−H);

^{1}H NMR (400 MHz, DMSO-d_6) δ 12.76 (s, 1H, −NH), 8.34 (s, 1H, 6-CH), 7.81−7.80 (d, 1H, ^3J = 1.6 Hz, 3′-H), 7.67−7.65 (d, 2H, ^3J = 5.2 Hz, 2″,6″-H), 7.60−7.54 (m, 2H, 3″,5″-H), 7.47−7.46 (d, 1H, ^3J = 2.8 Hz, 5′-H), 7.14−7.12 (dd, 1H, J = 4.8 Hz, J = 3.6 Hz, 4′-H), 2.06 (s, 3H, 4-Me).

^{13}C NMR (101 MHz) δ: 183.3, 170.1, 158.7, 149.5, 138.7, 138.4, 135.0, 131.0, 130.3, 129.5, 129.1, 128.0, 17.0.

HRMS (ESI): m/z calcd for $C_{16}H_{11}Cl_2N_3OS_2$: 394.9721; found: 395.9720 $[M + H]^+$.

(E)-(4-methyl-2-(2-(thiophen-2-ylmethylene)hydrazinyl)-thiazol-5-yl)(thiophen-2-yl)methanone (4h). Dark Brown Solid. mp. 179 °C; yield: 78%; IR (KBr) ν_{max} (cm^{-1}): 1558 (C═O), 1605 (C═N), 3290 (N−H);

^{1}H NMR (400 MHz, DMSO-d_6) δ 12.64 (s, 1H, −NH), 8.33 (s, 1H, 6-CH), 8.01−7.99 (dd, 1H, J = 4.8 Hz, J = 1.0 Hz, 3″-H), 7.90−7.88 (dd, 1H, J = 4.0 Hz, J = 1.0 Hz, 5″-H), 7.66−7.65 (d, 1H, ^3J = 5.2 Hz, 3′-H), 7.46−7.45 (d, 1H, ^3J = 2.8 Hz, 5′-H), 7.28−7.26 (dd, 1H, J = 5.2 Hz, J = 4.0 Hz, 4″-H), 7.15−7.12 (dd, 1H, J = 5.2 Hz, J = 3.6 Hz, 4′-H), 2.50 (s, 3H, 4-Me).

^{13}C NMR (101 MHz) δ: 177.1, 168.9, 145.0, 140.4, 139.7, 138.5, 133.7, 132.0, 130.6, 128.8, 128.4, 128.0, 18.4.

HRMS (ESI): m/z calcd for $C_{14}H_{11}N_3OS_3$: 333.0064; found: 334.0060 $[M + H]^+$.

(E)-(2-(2-(furan-2-ylmethylene)hydrazinyl)-4-methylthiazol-5-yl)(phenyl)methanone (4i). Greenish Solid. mp. 201 °C; yield: 83%; IR (KBr) ν_{max} (cm^{-1}): 1566 (C═O), 1643 (C═N), 3140 (N−H);

^{1}H NMR (400 MHz, DMSO-d_6) δ 12.52 (s, 1H, −NH), 7.92 (s, 1H, 6-CH), 7.77−7.74 (m, 1H, 3′-H), 7.61−7.59 (m, 2H, 2″,6″-H), 7.53−7.50 (m, 1H, 4″-H), 7.46−7.42 (m, 2H, 3″,5″-H), 6.82−6.81 (m, 1H, 5′-H), 6.54−6.53 (m, 1H, 4′-H), 2.22 (s, 3H, 4-Me).

^{13}C NMR (101 MHz) δ: 186.9, 169.6, 148.9, 145.2, 140.5, 135.1, 131.5, 128.5, 127.6, 114.0, 112.2, 18.3.

HRMS (ESI): m/z calcd for $C_{16}H_{13}N_3O_2S$: 311.0728; found: 312.0720 $[M + H]^+$.

(E)-(2-(2-(furan-2-ylmethylene)hydrazinyl)-4-methylthiazol-5-yl)(p-tolyl)methanone (4j). Brownish Solid. mp. 220.5 °C; yield: 80%; IR (KBr) ν_{max} (cm^{-1}): 1597 (C═O), 1659 (C═N), 3271 (N−H);

^{1}H NMR (400 MHz, DMSO-d_6) δ 12.62 (s, 1H, −NH), 8.01−7.99 (m, 3H, 6,2″,6″-H), 7.90−7. 86 (m, 2H, 3″,5″-H),

https://doi.org/10.1021/acsomega.4c04924
ACS Omega 2024, 9, 38832−38845

7.25−7.27 (m, 1H, 3′-H), 6.93−6.92 (m, 1H, 5′-H), 6.65−6.63 (m, 1H, 4′-H), 2.51 (s, 6H, 4,4″-Me).

^{13}C NMR (101 MHz) δ: 177.0, 169.1, 148.8, 145.3, 145.1, 135.2, 133.7, 132.2, 132.0, 128.4, 114.1, 112.3, 18.7, 18.5.

HRMS (ESI): *m*/*z* calcd for $C_{17}H_{15}N_3O_2S$: 325.0885; found: 326.0884 $[M + H]^+$.

(E)-(2-(2-(furan-2-ylmethylene)hydrazinyl)-4-methylthiazol-5-yl)(4-methoxyphenyl)methanone (4k). Greenish Solid. mp. 201 °C; yield: 82%; IR (KBr) ν_{max} (cm^{-1}): 1558 (C═O), 1628 (C═N), 3155 (N−H);

^{1}H NMR (400 MHz, DMSO-d_6) δ 12.49 (s, 1H, −NH), 7.98 (s, 1H, 6-CH), 7.82 (d, 1H, *J* = 1.2 Hz, 3′-H), 7.73−7.70 (m, 2H, 2″,6″-H), 7.07−7.05 (m, 2H, 3″,5″-H), 6.89−6.88 (d, 1H, ^3J = 3.2 Hz, 5′-H), 6.63−6.61 (dd, 1H, *J* = 3.6 Hz, *J* = 2.0 Hz, 4′-H), 3.85 (s, 3H, 4″-OMe), 2.33 (s, 3H, 4-Me).

^{13}C NMR (101 MHz) δ: 185.7, 168.9, 162.1, 148.9, 145.1, 132.6, 130.3, 113.8, 113.7, 112.2, 55.4, 18.3.

HRMS (ESI): *m*/*z* calcd for $C_{17}H_{15}N_3O_3S$: 341.0834; found: 342.0831 $[M + H]^+$.

(E)-(2,4-dichlorophenyl)(2-(2-(furan-2-ylmethylene)-hydrazinyl)-4-methylthiazol-5-yl)methanone (4l). Gray Colored Solid. Mp. 176 °C; Yield: 80%; IR (KBr) ν_{max} (cm^{-1}): 1566 (C═O), 1598 (C═N), 3186 (N−H);

^{1}H NMR (400 MHz, DMSO-d_6) δ 12.76 (s, 1H, −NH), 8.02 (s, 1H, 6-CH), 7.85−7.84 (d, 1H, *J* = 1.6 Hz, 6″-H), 7.81−7.80 (d, 1H, *J* = 1.6 Hz, 5″-H), 7.58−7.57 (m, 2H, 3″,3′-H), 6.94−6.93 (d, 1H, ^3J = 3.2 Hz, 5′-H), 6.64−6.62 (dd, 1H, *J* = 3.6 Hz, *J* = 2.0 Hz, 4′-H), 2.12 (s, 3H, 4-Me).

^{13}C NMR (101 MHz) δ 183.7, 170.7, 148.9, 145.7, 139.0, 136.6, 136.3, 135.4, 130.6, 129.7, 128.3, 115.0, 112.7, 17.7.

HRMS (ESI): *m*/*z* calcd for $C_{16}H_{11}Cl_2N_3O_2S$: 378.9949; found: 380.0011 $[M + H]^+$.

(E)-(2-(2-((1H-indol-3-yl)methylene)hydrazinyl)-4-methylthiazol-5-yl)(phenyl)methanone (4m). Dark Brown Solid. mp. 229 °C; yield: 88%; IR (KBr) ν_{max} (cm^{-1}): 1566 (C═O), 1628 (C═N), 3291 (N−H);

^{1}H NMR (400 MHz, DMSO-d_6) δ 12.40 (s, 1H, −NH), 11.66 (d, 1H, *J* = 4.0 Hz, 3′-NH), 8.36−8.35 (s, 1H, 6-CH), 8.16−8.13 (m, 1H, 2′-H), 7.88−7.85 (m, 1H, 7′-H), 7.71−7.68 (m, 2H, 2″,6″-H), 7.62−7.52 (m, 3H, 3″,5″,4″-H), 7.49−7.45 (m, 1H, 4′-H), 7.25−7.17 (m, 2H, 5′,6′-H), 2.22 (s, 3H, 4-Me).

^{13}C NMR (101 MHz) δ: 187.0, 142.9, 140.6, 137.1, 131.3, 130.8, 128.4, 128.1, 127.7, 124.0, 122.7, 121.5, 120.7, 112.0, 111.2, 18.7.

HRMS (ESI): *m*/*z* calcd for $C_{20}H_{16}N_4OS$: 360.1045; found: 361.1044 $[M + H]^+$.

(E)-(2-(2-((1H-indol-3-yl)methylene)hydrazinyl)-4-methylthiazol-5-yl)(p-tolyl)methanone (4n). Greenish Solid. mp. 243 °C; yield: 90%; IR (KBr) ν_{max} (cm^{-1}): 1574 (C═O), 1604 (C═N), 3178 (N−H);

^{1}H NMR (400 MHz, DMSO-d_6) δ 12.34 (s, 1H, −NH), 11.63 (d, 1H, *J* = 2.0 Hz, 3′-NH), 8.34 (s, 1H, 6-CH), 8.15−8.14 (d, 1H, *J* = 2.1 Hz, 2′-H), 7.85 (d, 1H, *J* = 2.4 Hz, 7′-H), 7.62−7.60 (d, 2H, *J* = 8.0 Hz, 2″,6″-H), 7.47−7.45 (m, 1H, 4′-H), 7.35−7.33 (d, 2H, *J* = 8.0 Hz, 3″,5″-H), 7.24−7.15 (m, 2H, 5′,6′-H), 2.40 (s, 3H, 4″-Me), 2.23 (s, 3H, 4-Me).

^{13}C NMR (101 MHz) δ: 186.8, 141.5, 137.7, 137.1, 130.7, 128.9, 128.0, 124.0, 122.7, 121.5, 120.7, 112.0, 111.3, 21.1, 18.7.

HRMS (ESI): *m*/*z* calcd for $C_{21}H_{18}N_4OS$: 374.1201; found: 375.1198 $[M + H]^+$.

(E)-(2-(2-((1H-indol-3-yl)methylene)hydrazinyl)-4-methylthiazol-5-yl)(2-methoxyphenyl)methanone (4o). Brownish Solid. mp. 212 °C; yield: 85%; IR (KBr) ν_{max} (cm^{-1}): 1566 (C═O), 1610 (C═N), 3155 (N−H);

^{1}H NMR (400 MHz, DMSO-d_6) δ 12.35 (s, 1H, −NH), 11.64−11.62 (d, 1H, *J* = 6.4 Hz, 3′-NH), 8.34 (s, 1H, 6-CH), 8.16−8.12 (m, 1H, 2′-H), 7.86−7.83 (m, 1H, 7′-H), 7.50−7.43 (m, 2H, 2″,6″-H), 7.27−7.12 (m, 4H, 4′,5′,3″,5″-H), 7.08−7.02 (m, 1H, 6′-H), 3.76 (s, 3H, 4″-OMe), 1.97 (s, 3H, 4-Me).

^{13}C NMR (101 MHz) δ: 185.7, 155.6, 143.1, 142.7, 137.1, 131.1, 130.8, 130.5, 127.5, 124.0, 122.7, 121.5, 120.7, 120.6, 112.0, 111.7, 111.3, 55.5, 17.3.

HRMS (ESI): *m*/*z* calcd for $C_{21}H_{18}N_4O_2S$: 390.1150; found: 391.1149 $[M + H]^+$.

(E)-(2-(2-((1H-indol-3-yl)methylene)hydrazinyl)-4-methylthiazol-5-yl)(3-methoxyphenyl)methanone (4p). Creamy White Solid. mp. 234 °C; yield: 82%; IR (KBr) ν_{max} (cm^{-1}): 1574 (C═O), 1636 (C═N), 3186 (N−H);

^{1}H NMR (400 MHz, DMSO-d_6) δ 12.40 (s, 1H, −NH), 11.64 (s, 1H, 3′-NH), 8.34 (s, 1H, 6-CH), 8.14−8.12 (d, 1H, *J* = 7.6 Hz, 2′-H), 7.88−7.85 (m, 1H, 7′-H), 7.47−7.43 (m, 2H, 2″,6″-H), 7.26−7.24 (m, 1H, 4′-H), 7.21−7.19 (m, 2H, 3″,5″-H), 7.18−7.15 (m, 2H, 5′,6′-H), 3.83 (s, 3H, 4″-OMe), 2.24 (s, 3H, 4-Me).

^{13}C NMR (101 MHz) δ: 186.5, 159.1, 142.0, 137.1, 130.8, 129.6, 123.9, 122.7, 121.4, 120.7, 119.9, 117.3, 112.4, 112.0, 111.2, 55.3, 18.8.

HRMS (ESI): *m*/*z* calcd for $C_{21}H_{18}N_4O_2S$: 390.1150; found: 391.1149 $[M + H]^+$.

(E)-(2-(2-((1H-indol-3-yl)methylene)hydrazinyl)-4-methylthiazol-5-yl)(4-fluorophenyl)methanone (4q). Brown Solid. Mp. 217.5 °C; yield: 86%; IR (KBr) ν_{max} (cm^{-1}): 1597 (C═O), 1628 (C═N), 3240 (N−H);

^{1}H NMR (400 MHz, DMSO-d_6) δ 12.39 (s, 1H, −NH), 11.64 (s, 1H, 3′-NH), 8.35 (s, 1H, 6-CH), 8.15−8.13 (d, 1H, *J* = 7.2 Hz, 2′-CH), 7.87−7.86 (m, 1H, 7′-H), 7.80−7.77 (m, 2H, 2″,6″-H), 7.47−7.45 (m, 1H, 4′-H), 7.39−7.34 (m, 2H, 3″,5″-H), 7.24−7.17 (m, 2H, 5′,6′-H), 2.23 (s, 3H, 4-Me).

^{13}C NMR (101 MHz) δ: 185.6, 169.8, 165.0, 162.6, 142.8, 137.1, 137.0, 130.9, 130.6, 130.5, 124.0, 122.7, 121.5, 120.8, 115.6, 115.3, 112.0, 111.2, 18.8.

HRMS (ESI): *m*/*z* calcd for $C_{20}H_{15}FN_4OS$: 378.0951; found: 379.0950 $[M + H]^+$.

(E)-(2-(2-((1H-indol-3-yl)methylene)hydrazinyl)-4-methylthiazol-5-yl)(4-chlorophenyl)methanone (4r). Creamish White Solid. mp. 210 °C; yield: 83%; IR (KBr) ν_{max} (cm^{-1}): 1574 (C═O), 1612 (C═N), 3283 (N−H);

^{1}H NMR (400 MHz, DMSO-d_6) δ 12.45 (s, 1H, −NH), 11.66 (d, 1H, *J* = 2.0 Hz, 3′-NH), 8.35 (s, 1H, 6-CH), 8.15−8.13 (m, 1H, 2′-CH), 7.87−7.86 (d, 1H, *J* = 2.4 Hz, 7′-H), 7.74−7.70 (m, 2H, 2″,6″-H), 7.62−7.58 (m, 2H, 3″,5″-H), 7.48−7.45 (m, 1H, 4′-H), 7.25−7.17 (pd, 2H, *J* = 7.2 Hz, *J* = 1.6 Hz, 5′,6′-H), 2.22 (s, 3H, 4-Me).

^{13}C NMR (101 MHz) δ 185.6, 142.9, 139.2, 137.1, 136.0, 130.9, 129.7, 128.6, 124.0, 122.7, 121.5, 120.8, 112.0, 111.2, 18.9.

HRMS (ESI): *m*/*z* calcd for $C_{20}H_{15}ClN_4OS$: 394.0655; found: 395.0651 $[M + H]^+$.

(E)-(2-(2-((1H-indol-3-yl)methylene)hydrazinyl)-4-methylthiazol-5-yl)(2,4-dichlorophenyl)methanone (4s). Dark Green Solid. mp. 239.5 °C; yield: 78%; IR (KBr) ν_{max} (cm^{-1}): 1578 (C═O), 1604 (C═N), 3188 (N−H);

https://doi.org/10.1021/acsomega.4c04924
ACS Omega 2024, 9, 38832−38845

^{1}H NMR (400 MHz, DMSO-d_6) δ 12.62 (s, 1H, −NH), 11.69 (d, 1H, J = 2.0 Hz, 3′-NH), 8.38 (s, 1H, 6-CH), 8.17−8.14 (m, 1H, 2′-CH), 7.88−7.87 (d, 1H, J = 3.2 Hz, 7′-H), 7.81−7.80 (d, 1H, J = 2.0 Hz, 6″-H), 7.60−7.54 (m, 2H, 3″,5″-H), 7.49−7.47 (m, 1H, 4′-H), 7.25−7.21 (m, 2H, 5′,6′-H), 2.57 (s, 3H, 4-Me).

^{13}C NMR (101 MHz) δ: 183.1, 179.5, 143.7, 138.8, 137.2, 134.9, 131.3, 130.4, 129.6, 129.4, 128.1, 124.0, 122.9, 121.6, 120.9, 112.1, 111.2, 17.8.

HRMS (ESI): m/z calcd for $C_{20}H_{14}Cl_2N_4OS$: 428.0265; found: 429.0341 $[M + H]^+$.

Cytotoxicity Viability Assay. A total of 50,000 MOLT-4 cells were seeded into a 96-well plate and treated with various compounds at a final concentration of 10 μM. The cells were then incubated for 48 h. To assess cell viability, an MTT cell proliferation kit from ATCC (no. 30e1010K) was employed. In brief, 10 μL of MTT reagent was added to each well, and the cells were placed back in the incubator for 4 h. Subsequently, 100 μL of detergent (from the kit) was added, and absorbance data were collected at 570 nm using a BioTek Synergy 2 spectrophotometer.

The obtained data were calculated as the percentage of cell survival using the following formula

$$\text{Percentage of Cell Survival} = \left(\text{Absorbance of treated}\frac{\text{Cells}}{\text{Absorbance}}\text{of untreated Cells}\right) \times 100$$

Cells were treated with varying concentrations of respective compounds followed by regular MTT assay, and IC_{50} was calculated using graph pad prism software.

Effects on Morphological Attributes. 7000 MCF-7 cells were incubated in a 96-well plate overnight before exposure to **4m**, **4n**, **4r**, and **4p** at a final concentration of 5 μM. After 24 h, the cells were examined at 20× magnification using a FLoid Imaging Station, Thermo-Scientific. To establish a positive control, doxorubicin was used at a concentration of 2 μM, while PBS was used as a negative control.

Caspase-3/7 Assay. In a 96-well plate, 50,000 MOLT-4 cells were plated and treated with **4m**, **4n**, and **4r** at a final concentration of 5 μM for 48 h. Following this, 100 μL of cells was transferred into a 96-well black plate and subjected to the Apo-ONE Homogeneous Caspase 3/7 Assay (Promega). Fluorescence (ex499/em520 nm) was measured every 30 min for 4 h.

Alteration to Assess Mitochondrial Membrane Potential. 100,000 MOLT-4 cells were plated in a 96-well plate and treated with a final concentration of **4m**, **4n**, **4r**, and **4k**. After 24 h, the cells were centrifuged for 10 min at 3000 rpm, media was removed, and 100 μL of 15 μM JC-10 (obtained from Santa Cruz Biotechnology) was resuspended into the wells and incubated for 45 min. The cells were observed under the ECHO Revolve fluorescence microscope using FITC and TRITC channels. 1 μM camptothecin was used as the positive control and PBS as the negative control.

mRNA Expression Using Quantitative RT-PCR. 300,000 MCF-7 cells were plated on a six-well plate and treated for 48 h. Total RNA was extracted with the TRIzol agent using ZYMO RESEARCH RNA MINIPREP KIT, and cDNA was synthesized using a SuperScript IV VILO Master Mix. The target gene was amplified by PCR with 40 cycles of denaturation at 95 °C for 15 s, annealing, and extension at 60 °C for 60 s. The relative mRNA level was calculated using the 2−ΔΔCt method. All data were normalized to the actin expression. Results were obtained from a QuantStudio 3 System.

Instigation of Cell Cycle Analysis Using Flow Cytometry. MOLT-4 cells were synchronized in the G_0/G_1 phase by serum deprivation with 0.2% FBS for 24 h. 5,000,000 MOLT-4 cells were treated with 0.5 μM camptothecin, 1 μM camptothecin, PBS, and 5 μM of **4m**, **4n**, and **4r** for 24 h. 1,000,000 cells were fixed with 70% ethanol and stained with propidium iodide and RNase solution for 15 min. Cell cycle results were read using an Attune NxT Flow Cytometer.

Tubulin Polymerization Assay. 10 μM of **4m**, **4n**, and **4r** was added to pure tubulin (1.2 mg/mL) protein for 5 min at room temperature in a 96-well plate, the reaction was initiated by adding polymerization buffer (as per a kit from Cytoskeleton; BK011P), and the reaction was monitored for change in fluorescence (Ex: 360 nm and Em: 420 nm) using a BioTek fluorimeter. Colchicine was used as a positive control inhibitor of tubulin polymerization. Taclitaxel was used to demonstrate how it stabilized tubulin polymerization.

■ ASSOCIATED CONTENT

Supporting Information

The Supporting Information is available free of charge at https://pubs.acs.org/doi/10.1021/acsomega.4c04924.

Additional experimental data (^{1}H, ^{13}C, HMBC, HSQC, NMR, and HRMS spectra) for final compounds (PDF)

■ AUTHOR INFORMATION

Corresponding Authors

Ranjana Aggarwal − *Department of Chemistry, Kurukshetra University, Kurukshetra, Haryana 136119, India; Council of Scientific and Industrial Research-National Institute of Science Communication and Policy Research, New Delhi 110012, India;* orcid.org/0000-0001-8848-9602; Phone: +91-9896740740; Email: ranjanaaggarwal67@gmail.com, ranjana67in@yahoo.com

Rachna Sadana − *Department of Natural Sciences, University of Houston, Houston, Texas 77002, United States;* Email: sadanar@uhd.edu

Authors

Prince Kumar − *Department of Chemistry, Kurukshetra University, Kurukshetra, Haryana 136119, India*

Suresh Kumar − *Department of Chemistry, Kurukshetra University, Kurukshetra, Haryana 136119, India*

Robert Lwanga − *Department of Natural Sciences, University of Houston, Houston, Texas 77002, United States*

Jude Campbell − *Department of Natural Sciences, University of Houston, Houston, Texas 77002, United States*

Vaishali Chaubal − *Department of Natural Sciences, University of Houston, Houston, Texas 77002, United States*

Complete contact information is available at: https://pubs.acs.org/10.1021/acsomega.4c04924

Notes

The authors declare no competing financial interest.

■ ACKNOWLEDGMENTS

We are highly thankful to the Council of Scientific and Industrial Research (CSIR), New Delhi, India for kindly

providing financial assistance for JRF & SRF to P.K. (Grant 09/105(0302)/2020-EMR-I). We also thank the UHD for financial assistance by providing the ORCA (Organized Research and Creative Activities) grant that supported biological assays.

REFERENCES

(1) Bray, F.; Ferlay, J.; Soerjomataram, I.; Siegel, R. L.; Torre, L. A.; Jemal, A. Global Cancer Statistics 2018: GLOBOCAN Estimates of Incidence and Mortality Worldwide for 36 Cancers in 185 Countries. *CA. Cancer J. Clin.* **2018**, *68* (6), 394−424.

(2) Aggarwal, R.; Kumar, P.; Jain, N.; Hooda, M.; Kumar, S.; Sadana, R.; Lwanga, R.; Guzman, A.; Chugh, H.; Chandra, R. Synthesis and In Vitro-In Silico Evaluation of Thiazolo-triazole Hybrids as Anticancer Candidates. *ChemistrySelect* **2023**, *8* (28), No. e202301368.

(3) Chen, D. S.; Mellman, I. Elements of Cancer Immunity and the Cancer-Immune Set Point. *Nature* **2017**, *541* (7637), 321−330.

(4) Sharma, P.; Hu-Lieskovan, S.; Wargo, J. A.; Ribas, A. Primary, Adaptive, and Acquired Resistance to Cancer Immunotherapy. *Cell* **2017**, *168* (4), 707−723.

(5) Brandes, B.; Hoenke, S.; Starke, N.; Serbian, I.; Deigner, H. P.; Al-Harrasi, A.; Csuk, R. Synthesis and Cytotoxicity of Apoptosis-Inducing N-Heterocyclic Triterpene Amides. *Eur. J. Med. Chem. Rep.* **2022**, *6* (December), 100085.

(6) Desai, S.; Desai, V.; Shingade, S. In-Vitro Anti-Cancer Assay and Apoptotic Cell Pathway of Newly Synthesized Benzoxazole-N-Heterocyclic Hybrids as Potent Tyrosine Kinase Inhibitors. *Bioorg. Chem.* **2020**, *94*, 103382.

(7) Kumar, A.; Singh, A. K.; Singh, H.; Vijayan, V.; Kumar, D.; Naik, J.; Thareja, S.; Yadav, J. P.; Pathak, P.; Grishina, M.; Verma, A.; Khalilullah, H.; Jaremko, M.; Emwas, A. H.; Kumar, P. Nitrogen Containing Heterocycles as Anticancer Agents: A Medicinal Chemistry Perspective. *Pharmaceuticals* **2023**, *16* (2), 299.

(8) Sağlık, B. N.; Kaya Çavuşoğlu, B.; Osmaniye, D.; Levent, S.; Acar Çevik, U.; Ilgın, S.; Özkay, Y.; Kaplancıklı, Z. A.; Öztürk, Y. In Vitro and in Silico Evaluation of New Thiazole Compounds as Monoamine Oxidase Inhibitors. *Bioorg. Chem.* **2019**, *85* (October 2018), 97−108.

(9) Yurttaş, L.; Çavuşoğlu, B. K.; Cantürk, Z. Novel 2-(2-Hydrazinyl)Thiazole Derivatives as Chemotherapeutic Agents. *Synth. Commun.* **2020**, *50* (20), 3072−3079.

(10) Maganti, L. H. B.; Ramesh, D.; Vijayakumar, B. G.; Khan, M. I. K.; Dhayalan, A.; Kamalraja, J.; Kannan, T. Acetylene Containing 2-(2-Hydrazinyl)Thiazole Derivatives: Design, Synthesis, and in Vitro and in Silico Evaluation of Antimycobacterial Activity against Mycobacterium Tuberculosis. *RSC Adv.* **2022**, *12* (14), 8771−8782.

(11) Morigi, R.; Locatelli, A.; Leoni, A.; Rambaldi, M. Recent Patents on Thiazole Derivatives Endowed with Antitumor Activity. *Recent Pat. Anti-Cancer Drug Discovery* **2015**, *10* (3), 280−297.

(12) Ayati, A.; Emami, S.; Asadipour, A.; Shafiee, A.; Foroumadi, A. Recent Applications of 1,3-Thiazole Core Structure in the Identification of New Lead Compounds and Drug Discovery. *Eur. J. Med. Chem.* **2015**, *97* (1), 699−718.

(13) Sharma, P. C.; Bansal, K. K.; Sharma, A.; Sharma, D.; Deep, A. Thiazole-Containing Compounds as Therapeutic Targets for Cancer Therapy. *Eur. J. Med. Chem.* **2020**, *188*, 112016.

(14) Gupta, V.; Kant, V. A Review on Biological Activity of Imidazole and Thiazole Moieties and Their Derivatives. *Sci. Int.* **2013**, *1* (7), 253−260.

(15) Sayed, A. R.; Gomha, S. M.; Taher, E. A.; Muhammad, Z. A.; El-Seedi, H. R.; Gaber, H. M.; Ahmed, M. M. One-Pot Synthesis of Novel Thiazoles as Potential Anti-Cancer Agents. *Drug Des., Dev. Ther.* **2020**, *14*, 1363−1375.

(16) Gümüş, M.; Yakan, M.; Koca, I. Recent Advances of Thiazole Hybrids in Biological Applications. *Future Med. Chem.* **2019**, *11* (15), 1979−1998.

(17) Tantawy, A. H.; El-Behairy, M. F.; Abd-Allah, W. H.; Jiang, H.; Wang, M. Q.; Marzouk, A. A. Design, Synthesis, Biological Evaluation, and Computational Studies of Novel Fluorinated Candidates as PI3K Inhibitors: Targeting Fluorophilic Binding Sites. *J. Med. Chem.* **2021**, *64* (23), 17468−17485.

(18) Althagafi, I.; El-Metwaly, N.; Farghaly, T. A. New Series of Thiazole Derivatives: Synthesis, Structural Elucidation, Antimicrobial Activity, Molecular Modeling and MOE Docking. *Molecules* **2019**, *24* (9), 1741.

(19) De Siqueira, L. R. P.; De Moraes Gomes, P. A. T.; De Lima Ferreira, L. P.; de Melo Rêgo, M. J. B.; Leite, A. C. L. Multi-Target Compounds Acting in Cancer Progression: Focus on Thiosemicarbazone, Thiazole and Thiazolidinone Analogues. *Eur. J. Med. Chem.* **2019**, *170*, 237−260.

(20) Szumilak, M.; Wiktorowska-Owczarek, A.; Stanczak, A. Hybrid Drugs—A Strategy for Overcoming Anticancer Drug Resistance? *Molecules* **2021**, *26* (9), 2601.

(21) Ivasiv, V.; Albertini, C.; Gonçalves, A. E.; Rossi, M.; Bolognesi, M. L. Molecular Hybridization as a Tool for Designing Multitarget Drug Candidates for Complex Diseases. *Curr. Top. Med. Chem.* **2019**, *19* (19), 1694−1711.

(22) Farghaly, T. A.; Abbas, E. M. H.; Al-Soliemy, A. M.; Sabour, R.; Shaaban, M. R. Novel Sulfonyl Thiazolyl-Hydrazone Derivatives as EGFR Inhibitors: Design, Synthesis, Biological Evaluation and Molecular Docking Studies. *Bioorg. Chem.* **2022**, *121*, 105684.

(23) Orujova, T.; Ece, A.; Akalın Çiftçi, G.; Özdemir, A.; Altıntop, M. D. A New Series of Thiazole-hydrazone Hybrids for Akt-targeted Therapy of Non-small Cell Lung Cancer. *Drug Dev. Res.* **2023**, *84* (2), 185−199.

(24) Altıntop, M. D.; Sever, B.; Akalın Çiftçi, G.; Özdemir, A. Design, Synthesis, and Evaluation of a New Series of Thiazole-Based Anticancer Agents as Potent Akt Inhibitors. *Molecules* **2018**, *23* (6), 1318.

(25) Aggarwal, R.; Hooda, M.; Kumar, P.; Kumar, S.; Singh, S.; Chandra, R. An Expeditious On-Water Regioselective Synthesis of Novel Arylidene-Hydrazinyl-Thiazoles as DNA Targeting Agents. *Bioorg. Chem.* **2023**, *136*, 106524.

(26) Mehmood, H.; Musa, M.; Woodward, S.; Hossan, M. S.; Bradshaw, T. D.; Haroon, M.; Nortcliffe, A.; Akhtar, T. Design, and Synthesis of Selectively Anticancer 4-Cyanophenyl Substituted Thiazol-2-Ylhydrazones. *RSC Adv.* **2022**, *12* (52), 34126−34141.

(27) El-Naggar, A. M.; El-Hashash, M. A.; Elkaeed, E. B. Eco-Friendly Sequential One-Pot Synthesis, Molecular Docking, and Anticancer Evaluation of Arylidene-Hydrazinyl-Thiazole Derivatives as CDK2 Inhibitors. *Bioorg. Chem.* **2021**, *108* (March), 104615.

(28) Gomha, S. M.; Abdelhady, H. A.; Hassain, D. Z. H.; Abdelmonsef, A. H.; El-Naggar, M.; Elaasser, M. M.; Mahmoud, H. K. Thiazole-Based Thiosemicarbazones: Synthesis, Cytotoxicity Evaluation and Molecular Docking Study. *Drug Des. Devel. Ther.* **2021**, *15*, 659−677.

(29) Aggarwal, R.; Hooda, M.; Kumar, P.; Jain, N.; Dubey, G. P.; Chugh, H.; Chandra, R. Visible-Light-Prompted Synthesis and Binding Studies of 5,6-Dihydroimidazo[2,1- b]Thiazoles with BSA and DNA Using Biophysical and Computational Methods. *J. Org. Chem.* **2022**, *87* (6), 3952−3966.

(30) Aggarwal, R.; Kumar, S.; Sadana, R.; Guzman, A.; Kumar, V. Multicomponent Synthesis, In Vitro Cytotoxic Evaluation and Molecular Modelling Studies of Polyfunctionalized Pyrazolo[3,4-b]Pyridine Derivatives against Three Human Cancer Cell Lines. *Synth. Commun.* **2021**, *51* (21), 3308−3324.

(31) Lossi, L. The Concept of Intrinsic versus Extrinsic Apoptosis. *Biochem. J.* **2022**, *479* (3), 357−384.

(32) Mithun, M. H.; Kar, A.; Prome, S. M.; Jahan, I.; Akter, A.; Hasan, S. E. A Comprehensive Review on Cell Death. *J. Knowl. Learn. Sci. Technol.* **2023**, *2* (3), 170−188.

(33) Hajibabaie, F.; Abedpoor, N.; Mohamadynejad, P. Types of Cell Death from a Molecular Perspective. *Biology* **2023**, *12* (11), 1426.

(34) Bertheloot, D.; Latz, E.; Franklin, B. S. Necroptosis, Pyroptosis and Apoptosis: An Intricate Game of Cell Death. *Cell. Mol. Immunol.* **2021**, *18* (5), 1106−1121.

https://doi.org/10.1021/acsomega.4c04924
ACS Omega 2024, 9, 38832−38845

(35) Banfalvi, G. Methods to Detect Apoptotic Cell Death. *Apoptosis* **2017**, *22* (2), 306−323.
(36) Guo, M.; Lu, B.; Gan, J.; Wang, S.; Jiang, X.; Li, H. Apoptosis Detection: A Purpose-Dependent Approach Selection. *Cell Cycle* **2021**, *20* (11), 1033−1040.
(37) McKenzie, B. A.; Fernandes, J. P.; Doan, M. A. L.; Schmitt, L. M.; Branton, W. G.; Power, C. Activation of the Executioner Caspases-3 and −7 Promotes Microglial Pyroptosis in Models of Multiple Sclerosis. *J. Neuroinflammation* **2020**, *17* (1), 253.
(38) Zhao, Y.; Zheng, Y.; Chen, X.; Du, R.; Yan, Z. Camptothecin Derivatives Induce Apoptosis and Inhibit Proliferation of Prostate Cancer PC-3M Cells through Downregulation of PI3K/Akt Signaling Pathway. *Phytochem. Lett.* **2021**, *46*, 79−89.
(39) Kilbride, S. M.; Prehn, J. H. M. Central Roles of Apoptotic Proteins in Mitochondrial Function. *Oncogene* **2013**, *32* (22), 2703−2711.
(40) Abate, M.; Festa, A.; Falco, M.; Lombardi, A.; Luce, A.; Grimaldi, A.; Zappavigna, S.; Sperlongano, P.; Irace, C.; Caraglia, M.; Misso, G. Mitochondria as Playmakers of Apoptosis, Autophagy and Senescence. *Semin. Cell Dev. Biol.* **2020**, *98*, 139−153.
(41) Qian, S.; Wei, Z.; Yang, W.; Huang, J.; Yang, Y.; Wang, J. The Role of BCL-2 Family Proteins in Regulating Apoptosis and Cancer Therapy. *Front. Oncol.* **2022**, *12*, 985363.
(42) Aggarwal, R.; Singh, G.; Sanz, D.; Claramunt, R. M.; Torralba, M. C.; Torres, M. R. NBS Mediated One-Pot Regioselective Synthesis of 2,3-Disubstituted Imidazo[1,2-a]Pyridines and Their Unambiguous Characterization through 2D NMR and X-Ray Crystallography. *Tetrahedron* **2016**, *72* (27−28), 3832−3838.

https://doi.org/10.1021/acsomega.4c04924
ACS Omega 2024, 9, 38832−38845